Control Engineering Practice 114 (2021) 104885

Contents lists available at ScienceDirect

Control Engineering Practice

journal homepage: www.elsevier.com/locate/conengprac

Model predictive control for amine-based CO_2 capture process with advanced flash stripper

Howoun Jung [a], Seongmin Heo [b,*], Jay H. Lee [a,*]

[a] Department of Chemical and Biomolecular Engineering, Korea Advanced Institute of Science and Technology, 291 Daehak-ro, Yuseong-gu, Daejeon 34141, Republic of Korea

[b] Department of Chemical Engineering, Dankook University, Yongin 16890, Republic of Korea

ARTICLE INFO

Keywords:
Post-combustion CO_2 capture
Advanced flash stripper
Model predictive control
Dynamic response analysis
Scenario study

ABSTRACT

Advanced flash stripper (AFS) has been suggested as a process alternative for conventional absorption-based post-combustion carbon capture process, which can significantly reduce the solvent regeneration energy. However, such reduction is enabled through energy integration achieved by two additional heat exchangers, which can pose serious challenges to the control and operation of carbon capture processes. For complex energy-integrated processes, simple decentralized control scheme, where multiple proportional–integral–derivative (PID) controllers are employed, typically shows limited control performances. Thus, this study aims to propose an effective control structure for the carbon capture process with AFS, which can regulate the process under various dynamic scenarios involving significant changes in operational variables such as flue gas flowrate and carbon capture rate. Specifically, a dynamic model for the post-combustion carbon capture process is built in *gPROMS,* where 30 wt% Monoethanolamine (MEA) solvent is used in the absorber. Then, step responses of the controlled outputs with respect to the manipulated and disturbance inputs are analyzed to characterize the dynamic behavior of such process. A model predictive control (MPC) strategy is proposed on the basis of the understanding from the analysis. Finally, the closed-loop performances of the proposed control strategy and decentralized PID controllers are compared to demonstrate the effectiveness of the MPC strategy. The MPC strategy demonstrates that it can track the set-point change at least 20 min faster than the PID strategies, and stabilize the stripper section about 200 min faster.

1. Introduction

Post-combustion CO_2 capture (PCC) process with aqueous amine solvents is now considered to be a matured technology, as it has been implemented for several commercial-scale applications (Koytsoumpa et al., 2018). A major obstacle, which still remains unsolved for such process, is its large energy consumption, which stems from the large amount of heat needed to regenerate CO_2 loaded solvent for recycle. The regeneration heat is typically provided by extracting steam from the power plant at which the PCC process is installed. However, the steam extraction can adversely affect the power plant, reducing the power generation efficiency by 10%–14% (Dave et al., 2011; Goto et al., 2013). Extensive research efforts, to this end, are going into the reduction of regeneration heat, which include the development of new single/blended/biphasic amine solvents (El Hadri et al., 2017; Muchan et al., 2017; Zhang et al., 2019), integration and intensification of the capture process configuration, (Cousins et al., 2011; Jung et al., 2015; Oh et al., 2020), and process optimization (Agbonghae et al., 2014; Li, Cousins et al., 2016).

Among such efforts, process integration focuses on developing energy-integrated process configurations utilizing stream split and vapor recompression, resulting in various configurations such as intercooling, cold solvent split (CSS) (Li, Leigh et al., 2016), lean vapor compression, rich vapor compression (Dubois & Thomas, 2018) and stripper overhead compression (Liang et al., 2015). Combinations of these configurations have also been proposed (Oh et al., 2020), one of which is advanced flash stripper (AFS), where the reduction of regeneration heat is mainly achieved in the stripper section (Lin et al., 2014). The PCC process with AFS (this process will be referred to as A-PCC process) maximizes the energy efficiency in the stripper section by replacing the conventional stripper with two heat exchangers and a flash drum. In this configuration, cold bypass, which is equivalent to CSS, and warm bypass streams are introduced to increase the temperature difference between the stripper inlet streams, so that the heat convection rate in the stripper can be enhanced. It has been shown that the AFS can save regeneration heat by as much as 18% compared to the conventional stripper with MEA (Rezazadeh et al., 2016). In addition, the operability of the AFS system with piperazine

* Corresponding authors.
E-mail addresses: smheo@dankook.ac.kr (S. Heo), jayhlee@kaist.ac.kr (J.H. Lee).

https://doi.org/10.1016/j.conengprac.2021.104885
Received 2 February 2021; Received in revised form 30 June 2021; Accepted 1 July 2021
Available online 14 July 2021

as an absorbent has been verified in a pilot plant study (Rochelle et al., 2019).

Another important feature, which PCC processes must pursue, is operational flexibility. Since the amounts of steam and flue gas supplied to the PCC process can significantly vary with the changes in the power plant, operating conditions of the PCC process must be able to adopt quickly and reliably to such changes to maintain the energy efficiency at a desired level (Bui et al., 2020; He et al., 2016). While energy-integrated configurations mentioned above provide significant economic benefits, they often exhibit complex process-level dynamics which can highly limit the performance of decentralized control structures (Heo & Daoutidis, 2016; Heo et al., 2014; Wu et al., 2020). Walters, Edgar et al. (2016) pointed out that, in the A-PCC process, the objective of strictly controlling the CO_2 capture rate can be hardly achieved with proportional–integral–derivative (PID) controllers, and concluded that an application of advanced control techniques should be considered to improve the flexibility and operability of the A-PCC process.

An application of model-based control techniques such as model predictive control (MPC) is an attractive option for a slow, interactive and constrained multi-input multi-output (MIMO) system such as PCC processes. Various versions of MPC, including linear (Hossein Sahraei & Ricardez-Sandoval, 2014; Luu et al., 2015; Zhang et al., 2016), nonlinear (He et al., 2018; Patron & Ricardez-Sandoval, 2020; Zhang et al., 2018), and economic MPC (Chan & Chen, 2018; Decardi-Nelson et al., 2018) have been successfully applied to PCC processes, demonstrating their superior control performances compared to the traditional PID controllers (Salvinder et al., 2019; Wu et al., 2020). However, these studies focused mainly on the conventional PCC process (this process will be referred to as C-PCC process), where energy integration is minimal.

To this end, this study specifically considers the development of MPC-based control strategy for the operational flexibility of the A-PCC process. First, we optimize the operating conditions of the C-PCC and A-PCC processes to obtain nominal operating points for the subsequent analysis. Using such points, the thermal efficiencies of both processes are compared to illustrate the benefits of the A-PCC process. Then, we select the optimal set of controlled variables for the A-PCC process via the self-optimizing control (Skogestad, 2000). After that, we design three different control strategies (two decentralized ones and a centralized one) for the flexible operation of the A-PCC process. Finally, we compare the control performances of three strategies under several dynamic scenarios, and provide detailed discussions on the results to highlight the advantages of MPC-based control strategy.

The contributions of this work are remarked as follows: (1) This study identifies the self-optimizing controlled variables in the presence of varying CO_2 capture rate or inlet stream condition, which reflects a practical PCC plant scenario. (2) This study investigates process dynamics and interaction between the process variables in the A-PCC process through the step response and relative gain array analysis. (3) This study demonstrates the improved control performance and operational flexibility that can be achieved by employing a MPC instead of simple PID controllers.

2. Process description and analysis

In this section, we first discuss the main features of the A-PCC process in comparison with the C-PCC process from a structural point of view, which is followed by the description of the dynamic process models we use to simulate the two processes. Using the dynamic models, steady-state simulations are performed to determine nominal operating conditions for both processes by minimizing a major energy efficiency indicator of PCC processes, namely the specific reboiler duty. Based on the steady-state simulation results, the energy efficiencies of both processes are compared to evaluate the benefits provided by the AFS.

2.1. Process description

Fig. 1 shows the process flow diagrams of the C-PCC and A-PCC processes, from which we can observe the shared and distinct features of the two processes. In both configurations, the amine solvent in the buffer tank flows into the absorber unit, and selectively absorbs CO_2 from the flue gas. The cleaned gas exits from the top of the absorber, while the amine solvent containing CO_2 leaves the absorber from the bottom, and goes into the stripping section for solvent regeneration. The CO_2 is stripped out from the heated solvent in the stripper column, and comes out of the system after being condensed. On the other hand, the regenerated solvent after the heat recovery is recycled, and stored in the buffer tank with water and amine makeup streams.

The major differences of the two processes lie in the stripping section. In the C-PCC process, the CO_2 rich solvent flows into the heat exchanger (HX) and then directly flows into the stripper. However, in the A-PCC process, several modifications to the heat integration scheme are considered for more efficient solvent regeneration. First, a small portion of the CO_2 rich solvent from the absorber (cold bypass) bypasses HX2 (which can be considered as the counterpart of HX in the C-PCC process) to recover heat from the hot vapor stream leaving the top of the stripper. The rest of the rich solvent flows into HX2 to be heated up to its bubble point. Then, a portion of the heated solvent (warm bypass) is drawn to be mixed with the preheated cold bypass and fed to the top of the stripper. These two bypass streams in the A-PCC process lower the inlet solvent temperature at the top of the stripper compared to the C-PCC process, which enhances the driving force for convective heat transfer, and the latent heat recovery in the stripper. The remaining boiling rich solvent from HX2 is further heated in HX3 and a steam heater, and then it is provided to the flash drum after being mixed with the stream from the bottom of the stripper. The rich solvent is regenerated in the recycle loop formed by the stripper column and the flash drum, and the regenerated solvent leaves the loop at the bottom of the flash drum to be recycled to the buffer tank after heat recovery. The steam heater and flash drum replace the reboiler in the C-PCC process, and thus contribute to the reduction in the CAPEX of the overall PCC process.

2.2. Dynamic process models

Mathematical models of the two PCC processes are constructed for the identification of optimal operating conditions, and process control studies. The most important units in the PCC process are the absorber and the stripper, where chemical absorption and desorption of the CO_2 occur. Due to the limited availability of pilot scale experimental data of the A-PCC process, the column model in Jung et al. (2020), which has been developed using the experimental data from a pilot scale C-PCC process (Notz et al., 2012), is employed to simulate the columns in both PCC processes. Despite the structural differences between the C-PCC and A-PCC processes, it is a reasonable approach since the optimal operating conditions are similar for the columns in both processes, as will be shown in the following section.

The column model in Jung et al. (2020) is a rigorous rate-based model, where the mass transfer phenomena enhanced by chemical reactions is described by the Maxwell–Stefan mass transfer model (Taylor & Krishna, 1993) and the reaction kinetic models (Hikita et al., 1977; Pinsent et al., 1956). In addition, the Kent–Eisenberg model (Kent & Elsenberg, 1976) is used to describe the chemical equilibrium and CO_2 partial pressure, while the electrolyte NRTL (non-random two liquid) thermodynamic model is used for the phase equilibrium. For the heat exchangers, a simple logarithm mean temperature difference (LMTD) approach is applied by assuming that the dynamics of heat exchangers are much faster than those of other process units, thus can be neglected. The dynamic model described above has been validated with the experimental data of a pilot scale C-PCC process, which utilizes 30wt% monoethanolamine (MEA) (Notz et al., 2012), and it was able

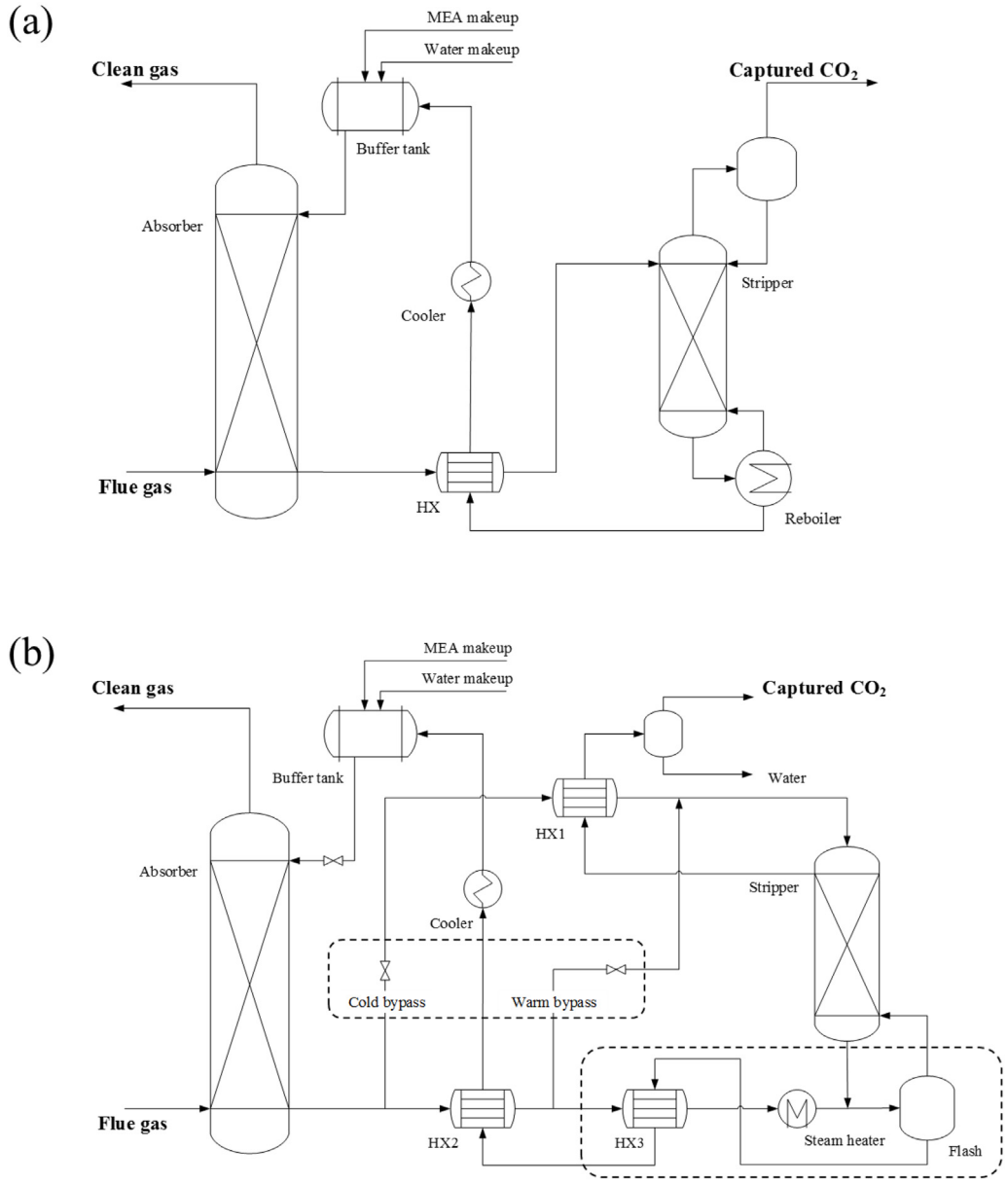

Fig. 1. Process flow diagrams of the amine-based PCC processes: (a) C-PCC process, (b) A-PCC process.

to predict the CO_2 capture rate and regeneration duty within an error range of ±10%. More details about the model can be found in Jung et al. (2020). The overall dynamic process model is simulated using the commercial software *gPROMS*.

2.3. Optimal operating conditions

Using the model mentioned above, steady-state simulations of C-PCC and A-PCC processes are performed to compare the energy efficiency of both processes, and to select optimal nominal operating conditions. The specifications for the inlet stream and process unit scale are first determined, and then the optimization problem is formulated to identify the optimal operating conditions.

The flue gas stream from a 300 MWe industrial scale coal-fired power plant is considered as the input stream to the PCC processes, and the 30wt% MEA solution is utilized as the absorbent. The flowrate and composition of the exhaust flue gas are calculated by the shortcut method of Mac Dowell and Shah (2013) as shown in Jung et al. (2020). 20% of excess air and 95% of combustion efficiency are assumed in this calculation. The unit specifications are roughly determined to meet the 70% flooding condition in each column in the C-PCC scheme. Table 1 shows the detailed information on the inlet stream and process unit configurations.

The regeneration heat duty required for a typical C-PCC process using an MEA solution accounts for approximately 80% of the total operating cost, which in turn corresponds to about 50% of the total annualized cost (Jung et al., 2015). There are two major indicators to measure the energy efficiency and operational performance of the PCC processes, specific regeneration duty (SRD) and CO_2 capture rate (η_{cap}), respectively, which are defined as follows:

$$SRD = \frac{\text{Regeneration duty}}{\text{Amount of captured } CO_2} [\text{MJ/kg } CO_2] \quad (1)$$

$$\eta_{cap} = \frac{\text{Amount of captured } CO_2}{\text{Amount of } CO_2 \text{ in inlet fluegas}} [\%] \quad (2)$$

For a fixed value of CO_2 capture rate, the lower SRD value translates into more energy savings. Hence, in this study, the energy-efficient operating conditions are defined as the conditions minimizing the SRD

Table 1
Inlet stream information and unit specifications.

Variable type	Variable	Value	Units
Inlet stream	Flue gas flowrate	364	[kg/s]
	CO_2 in flue gas	14.6	[mol%]
	H_2O in flue gas	8.6	[mol%]
Process unit	Absorber		
	- Height	22	[m]
	- Diameter	12	[m]
	- Packing type	Mellapak 250Y	
	Stripper		
	- Height	14	[m]
	- Diameter	8	[m]
	- Packing type	Mellapak 250Y	

value for a desired CO_2 capture rate, and an optimization problem can be formulated to find such conditions as below:

$$\begin{aligned} \min_{DV} \quad & SRD \\ \text{s.t.} \quad & f_{process}(U, Y, Z) = 0 \\ & \eta_{cap} = \eta_{cap,desired} \\ 500 \text{ kg/s} \le & F_{solv} \le 3000 \text{ kg/s} \\ 380 \text{ K} \le & T_{reb/fl} \le 393 \text{ K} \\ 10 \text{ kg/s} \le & F_{CBP} \le 500 \text{ kg/s} \\ 10 \text{ kg/s} \le & F_{WBP} \le 2000 \text{ kg/s} \end{aligned} \tag{3}$$

where DV represents the set of decision variables, while U and Y indicate the sets of process input and output variables, respectively. In the C-PCC process, the recirculated solvent flowrate (F_{solv}) and reboiler temperature (T_{reb}) are the decision variables (i.e. $DV_{C-PCC} = [F_{solv}, T_{reb}]$). On the other hand, in the A-PCC process, 4 decision variables are considered, which are the solvent flowrate (F_{solv}), flash temperature (T_{fl}), cold bypass flowrate (F_{CBP}) and warm bypass flowrate (F_{WBP}) (i.e. $DV_{A-PCC} = [F_{solv}, T_{fl}, F_{CBP}, F_{WBP}]$). U involves the inlet stream information such as the flue gas flowrate (F_{flue}) and compositions (y_{CO2}), while Y involves outlet stream information such as flowrate and composition of the streams from the top of the absorber and the stripper. Z indicates the set of remaining process parameters including unit configurations, and $f_{process}$ represents the steady-state version of the process model. The first equality constraint states that the steady-state version of the process model should be satisfied under the energy-efficient operating conditions, while the second equality constraint sets the CO_2 capture rate at the desired value, $\eta_{cap,desired}$. Inequality constraints are also included to restrict excessively low or high flowrates and temperature, which avoid abnormal process behaviors like flooding and ensure realistic operating conditions. The optimization problem in Eq. (3) is solved with the CVP_SS solver in *gPROMS*, which employs a sequential quadratic programming algorithm of NLPSQP.

Table 2 summarizes the optimization results for the C-PCC and A-PCC processes with the design specification provided in Table 1. The optimization results show that, under the energy-efficient operating conditions, the A-PCC process can lower the SRD by 21% compared to the C-PCC process, from 3.84 MJ/tCO_2 to 3.05 MJ/tCO_2. Generally, the SRD values of PCC processes are strongly affected by the solvent lean loading. For a typical MEA-based C-PCC process, the optimal lean loading is known to be around 0.2–0.28 CO_2mol/MEA mol, with the SRD value of 3.6–3.7 MJ/tCO_2, depending on the inlet stream conditions and system unit configurations (Agbonghae et al., 2014; Li, Cousins et al., 2016). On the other hand, in the case of an A-PCC process, the optimal SRD value is lower than that of C-PCC processes, and such value is achieved at a higher value of lean loading (0.324 in this study).

Table 2
Optimal operating condition of the C-PCC and A-PCC processes.

Variable type	Variable	C-PCC	A-PCC	Units
Design specification	CO_2 capture rate	90		[%]
	Stripper pressure	180		[kPa]
	Temperature approach	5		[K]
Decision variables	Solvent flowrate	1404	2388	[kg/s]
	Reboiler/Flash temperature	388.7	386.8	[K]
	Cold bypass flowrate	–	49	[kg/s]
	Warm bypass flowrate	–	1065	[kg/s]
Calculated variables	Regeneration duty	280	220	[MW]
	Lean loading	0.236	0.324	[mol/mol]
	Rich loading	0.493	0.477	[mol/mol]
	Cold bypass ratio	–	2.1	[%]
	Warm bypass ratio	–	44	[%]
	CO_2 purity	95.9	95.9	[%]
Objective value	SRD	3.84	3.05	[MJ/kgCO_2]

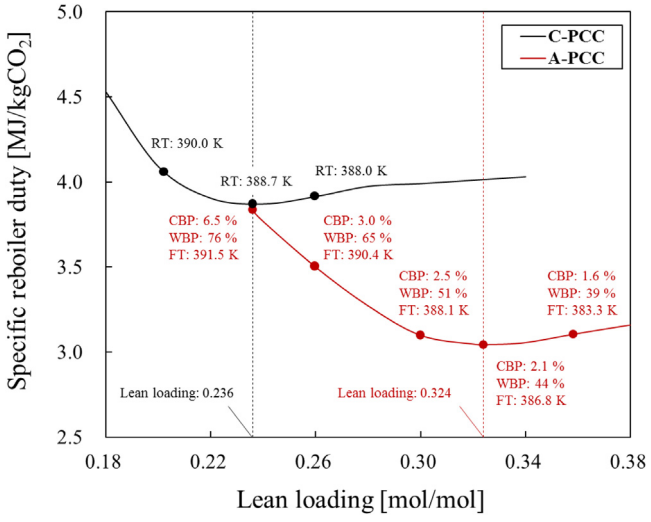

Fig. 2. Specific reboiler duty of the C-PCC (black) and A-PCC (red) processes with respect to the lean loading (CBP: cold bypass ratio, WBP: warm bypass ratio, RT/FT: reboiler/flash temperature).

Fig. 2 shows the optimized SRD values and operating conditions with the varying lean loading. For each condition, the reported bypass ratios are the proportions of the total recirculated solvent flowrate split into each bypass stream. At the lean loading of 0.236 (i.e. the optimal lean loading of the C-PCC process), two PCC processes have similar SRD values. However, note that the A-PCC process has much lower SRD values at higher lean loading conditions, compared to the C-PCC process. Also, it is notable that the optimal flash temperature, cold bypass ratio, and warm bypass ratio decrease as the lean loading increases. These simulation results show similar trends with the previous study of Rezazadeh et al. (2016), supporting the accuracy of the constructed process simulation model and the optimization results.

3. Closed-loop analysis of A-PCC process

Compared to the C-PCC process, the A-PCC process has two additional degrees of freedom, i.e., F_{CBP} and F_{WBP}. In the previous control studies, these free variables were fixed at constant flowrate ratios (Walters, Edgar et al., 2016), or used for the regulation of controlled outputs selected to maintain the process near the economic optimum via the so called self-optimizing control (Walters, Osuofa et al., 2016). However, these studies addressed only the stripper section of the A-PCC process, instead of the entire PCC process. Therefore, in this study, the self-optimizing control technique is applied to the entire A-PCC process in order to identify the best choices of controlled outputs to

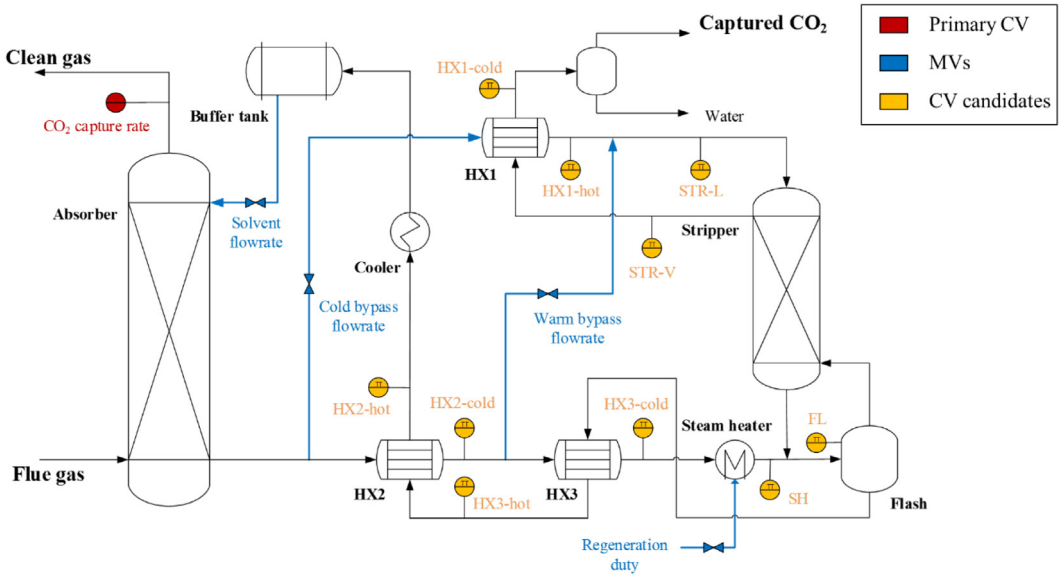

Fig. 3. Process flowsheet of A-PCC showing candidate controlled variables and manipulate variables.

Table 3
Considered changes in sensitivity analysis.

Condition	Changes	Nominal	Units
CO_2 capture rate	−10%p/+5%p	90	[%]
Inlet flue gas flowrate	−20%	364	[kg/s]
Inlet flue gas CO_2 concentration	+1%p	14.6	[mol%]

be regulated by the additional degrees of freedom. We then perform the step response analysis, and the relative gain array (RGA) analysis to obtain some insights into the dynamics and variable interactions of the A-PCC process. Based on the analysis results, we apply and compare two different PID control strategies and the MPC control strategy to the A-PCC process.

3.1. CV selection using self-optimizing control

Fig. 3 shows a process flowsheet of the A-PCC process, with 11 potential controlled variables (CVs) and 4 manipulated variables (MVs). The CO_2 capture rate is selected as a controlled variable, since it is the primary indicator of the performance of the PCC process. In addition, the temperature of the steam heater outlet or the flash drum should be maintained to guarantee a proper regeneration of the solvent. Among the 8 remaining potential CVs, we select 2 additional CVs using the self-optimizing control method, which can ensure a near-optimal operation of the process despite the major disturbances (chosen as the inlet flue gas flowrate and CO_2 concentration), and set point changes for the CO_2 capture rate. Also, in this selection, two additional candidates for CVs are considered, the temperature difference on the hot end of HX1 ($T_{STR-V} - T_{HX1-hot}$, defined as $TD1$) and the temperature difference at the top of the stripper ($T_{STR-V} - T_{STR-L}$, defined as $TD2$), which have been shown to be effective choices of CVs in Walters, Edgar et al. (2016).

Table 3 shows the ranges of the disturbances and the set point considered in this analysis. Variance in the CO_2 capture rate is first considered to change the CO_2 capture amount in relation to the energy price. The change in the flue gas flowrate represents a 20% decrease in the power plant load, while the change in CO_2 concentration corresponds to the case where the excess air supplied to the power plant decreases from 20% to 10%. By solving the optimization problem in Eq. (3) for different values of U and $\eta_{cap,desired}$, the sensitivity of the off-design values of the process variables with respect to the CO_2 capture rate set-point and flue gas conditions are evaluated. Here, off-design values imply the optimal values of the process variables when the process condition deviates from the nominal condition.

The sensitivity of off-design optimum values can be evaluated based on the calculated deviations from their nominal values:

$$\sigma = \left| y_{optimum} - y_{nominal} \right| \tag{4}$$

A small deviation means that the optimal value of the variable has low sensitivity to the condition changes, implying that keeping such variables constant can be helpful to maintain energy-efficient operating conditions in the flexible operation of the A-PCC process or the power plant.

Fig. 4 shows absolute deviations of the optimal values of the process variables in the face of +5%p and −10%p CO_2 capture rate changes, −20% flue gas flowrate change and +1%p flue gas CO_2 concentration change. For convenient analysis, all the deviation is normalized by dividing by the largest deviation values for each operating condition change. Note that $TD1$ and $TD2$ show the least deviations in the face of changes in the flue gas and CO_2 capture rate condition. This means that near-optimal operating conditions (in terms of minimizing SRD or energy consumption) can be achieved by keeping $TD1$ and $TD2$ at the nominal values, despite changes in the CO_2 capture rate or inlet flue gas condition. Therefore, from the viewpoint of minimizing the energy consumption, $TD1$ and $TD2$ are good choices of controlled variables.

Another issue concerns the temperatures of the steam heater (T_{sh}) and flash drum (T_{fl}). T_{sh} has much faster dynamics than T_{fl}, since the holdup of the steam heater is negligible and it is not directly influenced by the stripper temperature profile. However, the sensitivity analysis indicates that maintaining T_{sh} while letting T_{fl} drift could be problematic. In Fig. 4, T_{sh} has comparable sensitivities to changes in the capture rate or CO_2 concentration with T_{fl}, but it is much more sensitive to change in the flue gas flowrate. This means that selecting T_{sh} as a controlled variable can lead the A-PCC process to stray too far away from the optimal operating condition when the power plant load changes. Therefore, T_{fl} may be the more favorable controlled variable than T_{sh} if its set-point is to be fixed.

Based on the sensitivity analysis results, the CO_2 capture rate and the three least sensitive process variables of T_{fl}, $TD1$ and $TD2$ are selected as CVs of the A-PCC in this study.

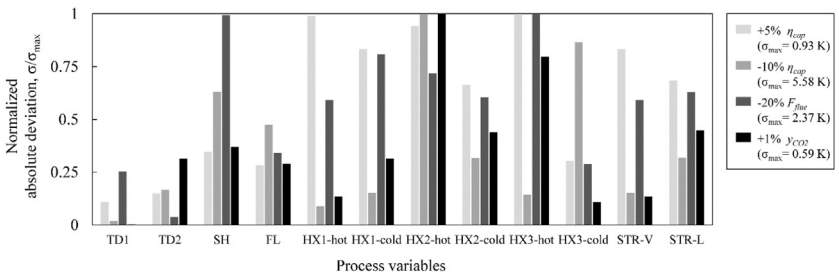

Fig. 4. Normalized sensitivity of off-design optimal values of the candidate CVs to changes in flue gas flowrate, CO_2 concentration and CO_2 capture rates.

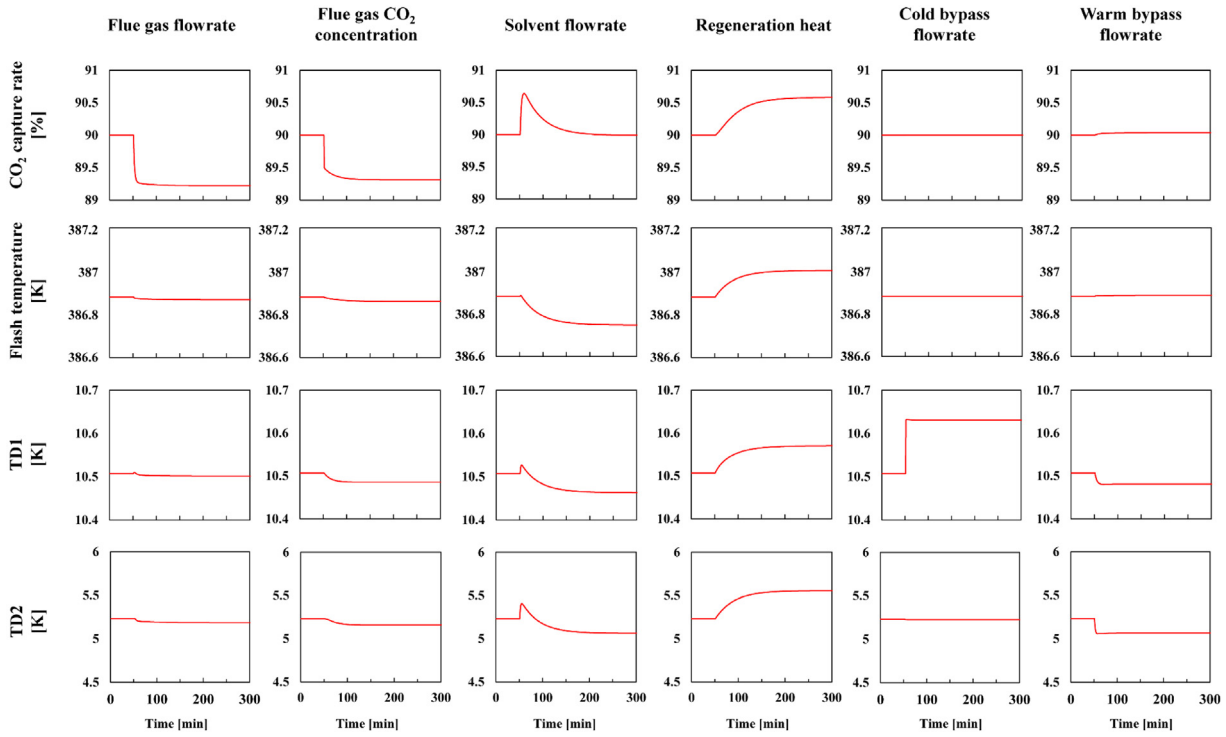

Fig. 5. Step responses of the controlled variables to +1% changes in the disturbance and manipulated variables.

3.2. Step response analysis and input–output pairing

Prior to designing the controllers, the degree of interactions among the process variables are analyzed via dynamic simulations. The step responses and the RGA are analyzed to gain insight into the dynamics of the A-PCC process and to examine the validity of using $TD1$ and $TD2$ as the controlled variables. The dynamic process model with the optimized nominal operating condition is used to obtain step responses of the A-PCC process. PID controllers are installed to maintain the solvent inventories in the process units (e.g. sump or flash drum), and it is assumed that the required flowrates of the makeup streams are calculated from the overall amine and water balances for a perfect makeup. Therefore, the analysis can be performed with respect to the main input variables of inlet flue gas flowrate (F_{flue}), CO_2 concentration (y_{CO2}), solvent flowrate (F_{solv}), regeneration heat (Q_{reg}), cold bypass flowrate (F_{CBP}) and warm bypass flowrate (F_{WBP}). Fig. 5 shows the step responses of the CVs when +1% step changes from the nominal values are introduced in the inputs at the 50 min mark.

The first two columns in Fig. 5 show the responses of CVs with respect to the disturbances in the flue gas flowrate and the CO_2 concentration. From the figure, it can be confirmed that changes in the flue gas conditions have a significant effect on the CO_2 capture rate. That is, a suitable control strategy is necessary to keep the CO_2 capture rate at the desired value in the face of varying flue gas flowrate and CO_2 composition.

The responses to the changes in MVs are shown in the 4 columns in the right-hand side of Fig. 5. Note that the responses to the solvent flowrate change show inverse response behavior. Initially, all the CVs increase rapidly, though the flash temperature and $TD1$ increase only by very small amounts. However, the flash temperature soon starts decreasing, and this causes an increase in the lean loading and decreases the CO_2 capture rate, $TD1$ and $TD2$ after some delay. Due to the nature of the recycled process, fast dynamics from step changes and slow dynamics from the recycled stream combine to give large and slow inverse responses. Those inverse responses, originating from the recycle stream, make it difficult to control the system tightly with decentralized controllers. It is also noticeable that all the responses to the regeneration duty change show very large time constants. This may limit the performance attainable by using feedback controllers only.

In the case of the responses to the bypass flowrate changes, it is observed that $TD2$ is only sensitive to the warm bypass flowrate change whereas $TD1$ is sensitive to both the cold and warm bypass flowrates, with a greater sensitivity to the warm bypass flowrate. That is, the two temperature differences are good choices for controlled variables since the cold and warm bypass flowrates have sufficient influences on them. Hence, the sensitivity analysis on the optimum off-design conditions (Section 3.1) and the step response analysis both indicate that using $TD1$ and $TD2$ as controlled variables is a sensible choice.

Relative gain array (RGA) analysis can give some insights on interactions among process variables to help select appropriate MV–CV

Table 4
Pairings of RGA-based and heuristics-based control structures.

Pairing	PID1 (RGA-based)		PID2 (Heuristics-based)	
	MVs	CVs	MVs	CVs
1	Q_{reg}	η_{cap}	F_{solv}	η_{cap}
2	F_{solv}	T_{fl}	Q_{reg}	T_{fl}
3	F_{CBP}	$TD1$	F_{CBP}	$TD1$
4	F_{WBP}	$TD2$	F_{WBP}	$TD2$

pairings in implementing single-input single-output (SISO) PID controllers. Based on the step response results, the RGA matrix (Λ) is computed as below:

$$\Lambda = \begin{array}{c} \\ \eta_{cap} \\ T_{fl} \\ TD1 \\ TD2 \end{array} \begin{array}{c} \begin{array}{cccc} F_{solv} & Q_{reg} & F_{CBP} & F_{WBP} \end{array} \\ \begin{bmatrix} -0.02 & 0.96 & 0.00 & 0.06 \\ 1.05 & -0.08 & 0.00 & 0.03 \\ 0.00 & 0.00 & 0.99 & 0.01 \\ -0.03 & 0.12 & 0.01 & 0.90 \end{bmatrix} \end{array} \tag{5}$$

Note that the pairings of $F_{solv} - \eta_{cap}$ and $Q_{reg} - T_{FL}$ have small but negative RGA values, implying that such pairing should be avoided as similar to the C-PCC case in the previous studies (Nittaya et al., 2014; Panahi & Skogestad, 2012). Although the negative pairings should be avoided from the viewpoint of steady-state interaction, the pairings of $F_{solv} - \eta_{cap}$ and $Q_{reg} - T_{fl}$, named hereafter the *heuristics-based pairings*, are one of the widely considered control structures (Mechleri et al., 2017; Montañés et al., 2017). This is because the physical distances between MVs and CVs for the other pairings of $F_{solv} - T_{fl}$ and $Q_{reg} - \eta_{cap}$ are quite large and consequently significant time-delays result to hamper effective control, while of the pairing of $F_{solv} - \eta_{cap}$ and $Q_{reg} - T_{fl}$ avoid such problem.

In the case of decentralized PID control, the pairings strongly affect the performance. Given this dilemma, both choices of pairings are considered in this study: the RGA-based pairings and the heuristics-based pairings. Each control strategy is named PID1 and PID2 respectively, and Table 4 shows the detailed parings of each control structure.

3.3. Control strategies

Three different control strategies for the A-PCC are formulated and compared in this study. The two PID-based decentralized control structures are introduced for comparison, and one model-based control structure is proposed to avoid the pairing issues and to overcome the limitation of the decentralized control. The ultimate objective of control is to quickly track the set-points when the flue gas flowrate and CO_2 concentration are disturbed, or the desired CO_2 capture rate changes.

A linear 6 × 4 input–output process model is first identified based on the result of the step response test, since the use of a linear model provides a good starting point when determining tuning parameters of the controllers. The identified linear model is given in discretized linear time-invariant (LTI) state–space form as follow:

$$\begin{aligned} x_{k+1} &= Ax_k + Bu_k + Ed_k \\ y_k &= Cx_k \end{aligned} \tag{6}$$

$$u_k \in [F_{solv}, Q_{reg}, F_{CBP}, F_{WBP}], \quad d_k \in [F_{flue}, y_{CO2}],$$
$$y_k \in [\eta_{cap}, T_{fl}, TD1, TD2]$$

Manipulated input variable vector u_k includes the solvent flowrate (F_{solv}), the regeneration duty (Q_{reg}), the cold bypass flowrate (F_{CBP}) and the warm bypass flowrate (F_{WBP}) while disturbance variable d_k includes the flue gas flowrate (F_{flue}) and the CO_2 concentration (y_{CO2}). Output variable vector y_k includes the CO_2 capture rate (η_{cap}), the flash temperature (T_{fl}), and the temperature difference 1 ($TD1$) and 2 ($TD2$). With this linear process model, controllers are initially tuned and they are retuned manually in the simulation of the rigorous nonlinear model. Since the rigorous dynamic model for the A-PCC is implemented in *gPROMS*, while all of the control strategies are constructed in *Matlab*, the *gO:Matlab* toolbox is used to run both the process model and the controllers simultaneously in the simulations.

3.3.1. PID controller

The pairings in Table 4 are used in the two different PID-based control strategies. The discrete-time PID controllers shown below are used:

$$U(z) = \left(P \cdot + I \cdot \frac{T_s z}{z-1} + D \cdot \frac{z-1}{T_s z} \right) (R(z) - Y(z)) \tag{7}$$

where R and Y represent the set-point and the process outputs in the z-domain respectively. T_s represents the sampling time (1 min) while P, I and D represent the tuning parameters. All the PID controllers are initially tuned with the Ziegler–Nichols step response method under the scenario of a 20% reduction in the flue gas flowrate. Since the A-PCC process has a large recycle stream, the controller parameters are initially tuned in a sequential manner and then are iteratively re-tuned. After that, they are manually fine-tuned to have robust closed-loop dynamics under other operating condition changes listed in Table 3. The tuned parameters for the PID-based controllers are shown in Table 5.

From Table 5, all the derivative terms are set to 0 in the PID2 strategy since the pairings of PID2 are physically very close and no dead-time is detected in the step responses. On the other hand, the pairings of PID1 (mainly $F_{solv} - T_{fl}$ and $Q_{reg} - \eta_{cap}$) have some time-delays due to their physical distances, and as a result, the derivate terms are set to have non-zero values to compensate for it.

3.3.2. Model predictive control

It is natural to consider the use of a model-based control technique for a MIMO system with slow dynamics with significant interactions like the PCC process. State–space MPC is considered in this study, and the identified linear process model is used as a predictive model in the MPC framework. To introduce an integral action in the MPC and correctly estimate the process state, the model is augmented with integrating states to represent the unmeasured output disturbance. Thus, the overall model is given in a LTI state–space form below:

$$\begin{aligned} \overline{x}_{k+1} &= \overline{A}\overline{x}_k + Bu_k + Ed_k = \begin{bmatrix} A & 0 \\ 0 & 0 \end{bmatrix} \begin{bmatrix} x \\ w_d \end{bmatrix}_k + Bu_k + Ed_k \\ y_k &= \overline{C}\overline{x}_k = \begin{bmatrix} C & I \end{bmatrix} \begin{bmatrix} x \\ w_d \end{bmatrix}_k \end{aligned} \tag{8}$$

where $\overline{x}_k$ is the augmented state vector including the process and disturbance states. w_d is the unmeasured disturbance, which is added to the output to compensate for the model-plant mismatch given the linear nature of the model. The augmented state vector $\overline{x}_k$ is estimated with the Kalman filter, of which both the state and output noise covariance matrices are initially set as the identity matrices.

The MPC algorithm solves the following optimization problem every minute (after a state update by the Kalman filter) so that it can minimize the tracking errors with the decision variables of the control input sequence in the predictive horizon:

$$\min_{\Delta u \in \mathbb{R}^{4 \times m}} \quad J = \sum_{i=1}^{p} (y_i - r_i)^T Q (y_i - r_i) + \sum_{i=1}^{m} \Delta u_i{}^T R \Delta u_i \tag{9}$$

The cost function J is the sum of the quadratic tracking errors and penalties on the control input change Δu. Here, Δu is considered only within the control horizon of m, since no input change is assumed beyond that point. To compute future output y along the predictive horizon, the predictive process model in Eq. (8) is used with the updated state and measured disturbance. During time integration of the predictive model, both measured and unmeasured disturbances, d_k and w_d, are considered to be constant. Also, set-point r is set to be constant along the prediction horizon, which means future reference trajectory

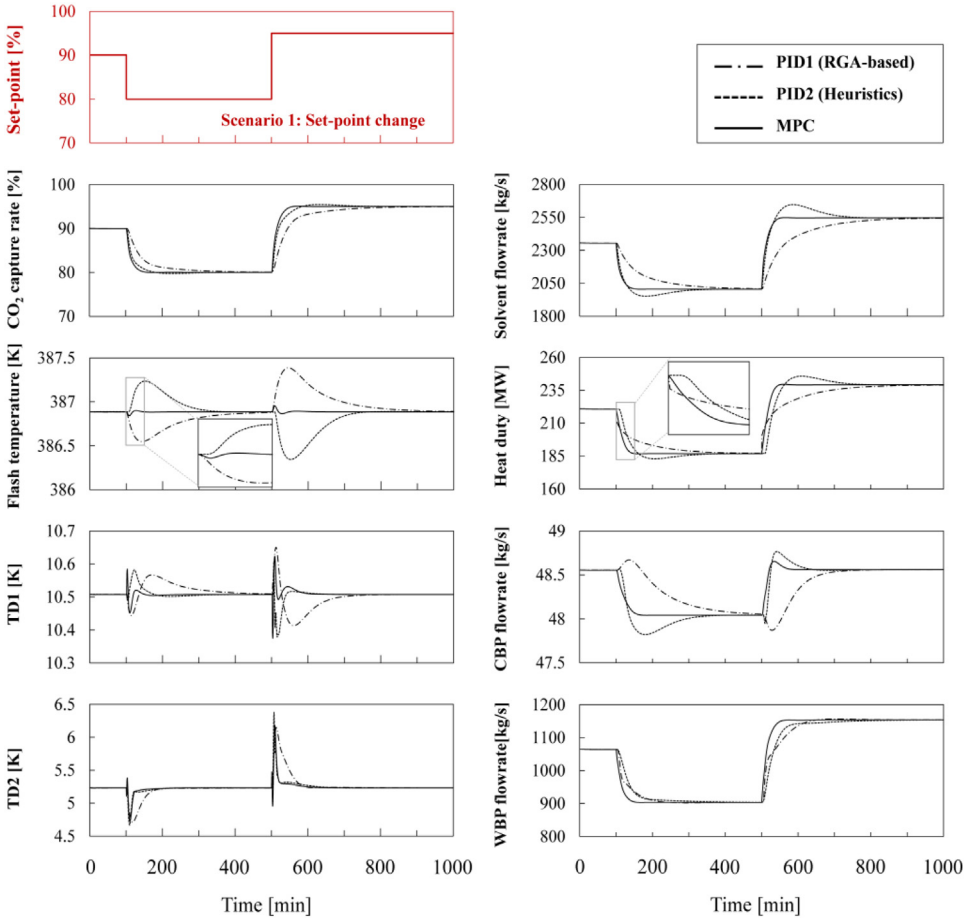

Fig. 6. Closed-loop responses of the three control strategies (PID1, PID2, MPC) for scenario 1 (left: control variables; right: manipulated variables).

Table 5
Tuning parameters for PID-based control strategies.

Pairings	PID1 (RGA-based)			PID2 (Heuristics-based)			Units
	P	I	D	P	I	D	
1	−326	−7.9	−161	5.3	3.1	0	[%/MW]/[%/(kg/s)]
2	0.92	0.07	1.50	63	0.93	0	[K/(kg/s]]/[K/MW]
3	0.10	0.10	0	0.10	0.10	0	[K/(kg/s)]
4	−13.3	−7.9	0	−20.8	−17.4	0	[K/(kg/s)]

is not used in solving the MPC problem. In this formulation, no terminal constraint for stabilizing the system is considered.

Due to the slow dynamics of the A-PCC process, the prediction horizon p and control horizon m are set to be 20 and 5 respectively. Despite the very slow inverse response observed in the step response of a SISO pair, these values are still reasonable as the effects of such dynamics can be minimized by tightly regulating the flash temperature under multivariable control (Wu et al., 2018). The control movements at every sampling time are limited to be within ±2% of the nominal values. The weighting parameters of Q and R are manually tuned as diag([1, 1, 0.5, 0.5]) and diag([10, 10, 10, 10]) respectively, considering both the robustness of the closed-loop dynamics and the order of priority on the control objectives. The optimization problem for the linear MPC, Eq. (9), can be solved with a typical QP solver. In our case, we use *KWIK* algorithm (Schmid & Biegler, 1994) for the QP solver.

4. Simulation results

This section evaluates three different control strategies with four different dynamic scenarios. Scenario 1, 2 and 3 include variance in CO_2 capture rate set-point and conditions of inlet flue gas respectively. Scenario 4 represents operation with a constraint on available regeneration heat, which the PCC processes may encounter during flexible operation. All of these dynamic scenarios are covered in Sections 4.1 to 4.4. Then, a comprehensive evaluation of each controller's performance is discussed.

4.1. Scenario 1: Changes in the CO_2 capture rate set-point

In Scenario 1, the CO_2 capture rate set-point changes from 90% to 80% and then to 95%. Since steam extracted from the power plant is likely to be the source of regeneration energy, the A-PCC process should be able to flexibly adjust its capture rate according to the electricity demand, in order to minimize CO_2 capture cost without compromising the satisfaction of the electricity demand. Fig. 6 shows the dynamic simulation results for Scenario 1.

Note that PID1 shows inferior control performance on the main control objective (e.g. tracking CO_2 capture rate set-point) compared to the other strategies. PID2 shows relatively good control performance exhibiting a slight overshoot or deviation, while the proposed MPC strategy can quickly track the set-point without any overshoot or prolonged deviation.

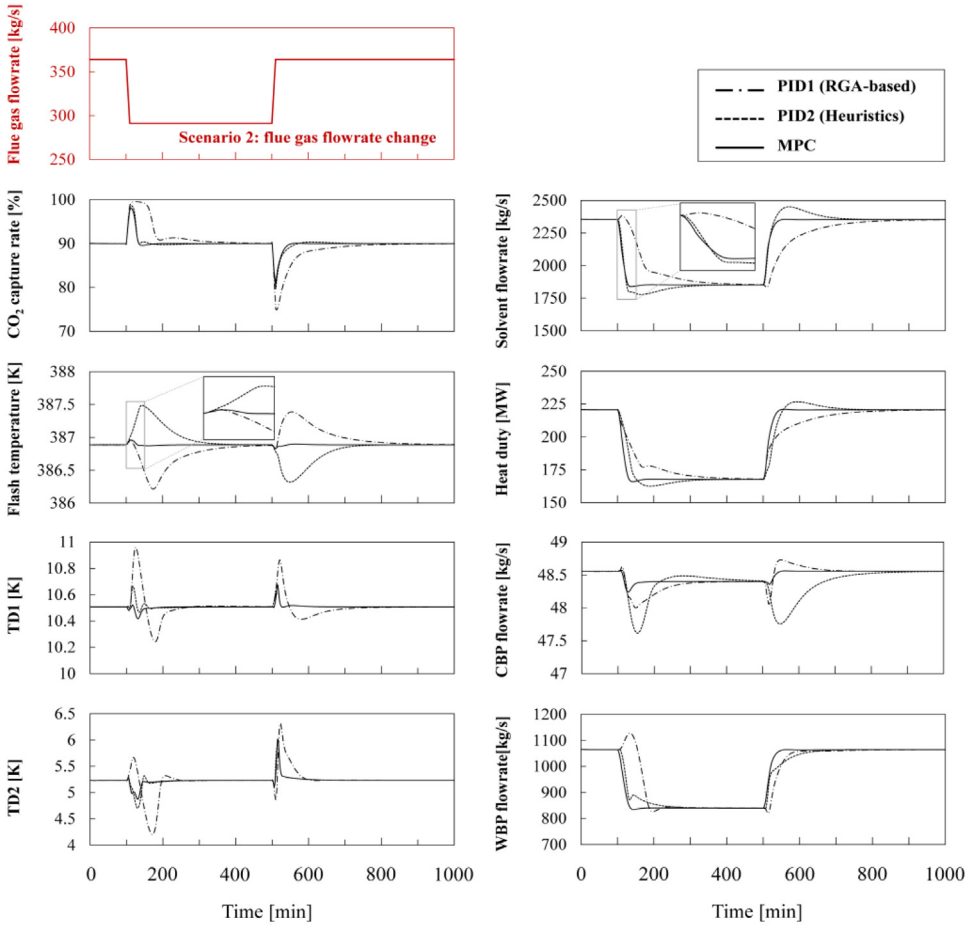

Fig. 7. Closed-loop responses of three control strategies (PID1, PID2, MPC) for scenario 2 (left: control variables; right: manipulated variables).

One remarkable observation is the closed-loop behavior of the flash temperature under the tested control strategies. It can be said that the MPC strategy shows good control performance by keeping the flash temperature almost constant. In the cases of the two PID control strategies, however, the closed-loop responses of the flash temperature are retarded to display significant excursions due to the slow, interactive dynamics of the A-PCC process due to the solvent holdup and bypasses in the stripper section. Note that all the MVs start to move when the set-point change occurs at the 100 min mark in the MPC strategy, while they do not in the PID-based strategies, probably due to the presence of inverse responses or delays. This suggests that the model-based multivariable controller is a more suitable choice for a slow, interactive system like the A-PCC process.

4.2. Scenario 2: Changes in the flue gas flowrate

Scenario 2 represents the partial-load operation of an integrated power plant. In the scenario, the flue gas flowrate decreases to 80% of the nominal value at 100 min and recovers to its nominal condition at 500 min. Since the flowrate of flue gas exhausted from the power plant is approximately proportional to the plant load (Mac Dowell & Shah, 2013), dynamic scenario 2 stands for a 20% reduction in the plant load and a subsequent recovery to the nominal load. A typical ramp rate for a coal-fired power plant of 2%/min is used in this scenario. Simulation results for scenario 2 are shown in Fig. 7.

Similar to the previous scenario 1, it can be seen that the control performance of PID1 is the worst when the power plant load change occurs. In particular, it cannot maintain the set-point of 90% capture rate for about 80 min and shows a large deviation when the flue gas flow rate decreases to 80% of the nominal value at 100 min. Also, it hardly tracks the CO_2 capture rate set-point when the plant load recovers at 500 min. PID2 and MPC show good control performance on the CO_2 capture rate in scenario 2 again.

Looking at the responses of flash temperature and solvent flowrate in Fig. 7 at the same time, PID1 exhibits small inverse responses in both the flash temperature and the paired manipulated variable of the solvent flowrate. Since the delayed movement of the solvent flowrate due to the inverse response causes another inverse response in $TD2$ (see dynamics of $F_{solv}-TD2$ pair in Fig. 5), the initial direction of the warm bypass flowrate is also inverted. Such delayed dynamics and complex interaction between the process variables make the A-PCC process very hard to control with the PID1 control strategy, even though it has the pairing choice recommended by the RGA. On the other hand, since there are no significant delays in the response of the pairings used in the PID2 strategy given the physical proximity, it can deliver satisfactory control performance on the CO_2 capture rate with just slight deviations as Fig. 7. The MPC controller shows fast and stable set-point tracking performance even under the disturbances in the flue gas flowrate.

4.3. Scenario 3: Changes in the flue gas CO_2 concentration

In addition to the flue gas flowrate, the CO_2 concentration in the exhausted flue gas can vary with the operating load. Scenario 3 considers this situation. Under the scenario, the CO_2 concentration of the flue gas changes by +1 mol%p at the 100 min mark and then recovers to its nominal value at the 500 min mark. Fig. 8 shows the disturbance and closed-loop simulation results for this scenario. Consistent with the previous cases, MPC shows the best control performance while PID1 shows the worst performance.

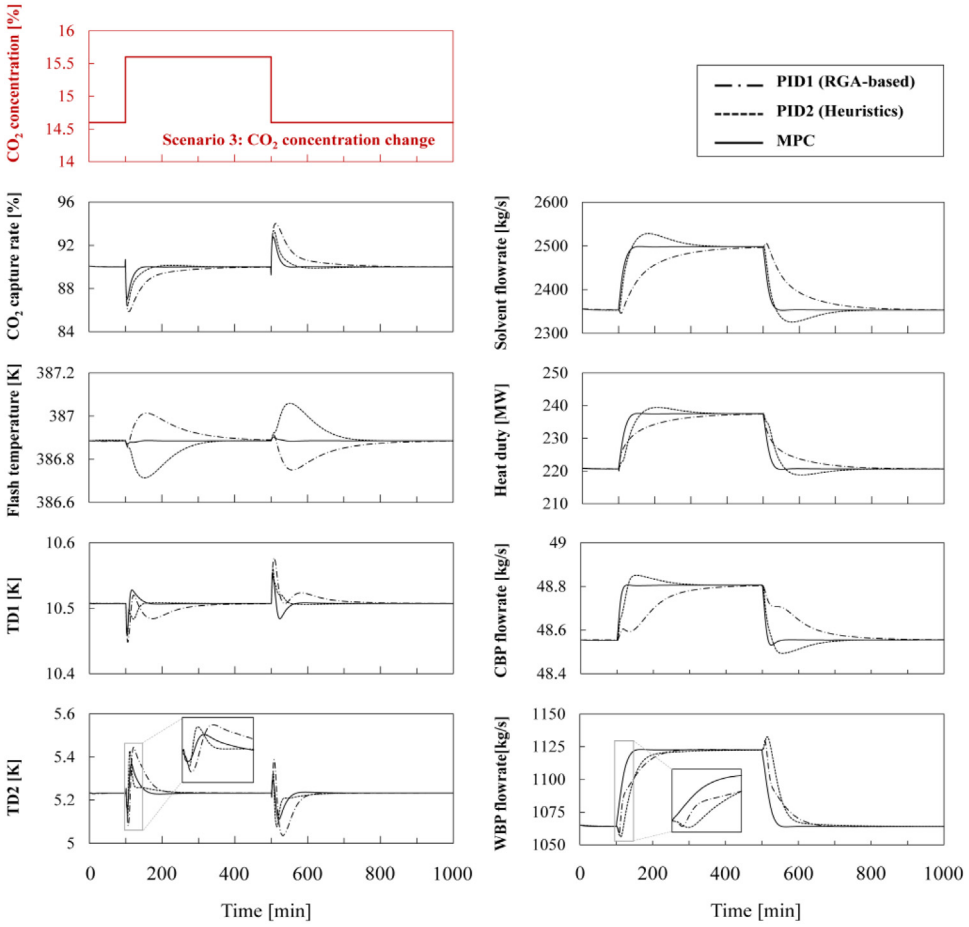

Fig. 8. Closed-loop responses of the three control strategies (PID1, PID2, MPC) for scenario 3 (left: control variables; right: manipulated variables).

One point to note is the movement of the warm bypass flowrate that the MPC makes. $TD2$ has slight inverse responses in its closed-loop dynamics, which causes the PID-based controller to act sluggishly as seen in Fig. 8. On the other hand, the MPC controller acts immediately and stabilizes the A-PCC much faster.

4.4. Scenario 4: Changes in the flue gas flowrate with limited regeneration heat

Flue gas flowrate changes due to partial operations of the power plant are major disturbances as previously described in Scenario 2. In general, however, the A-PCC is integrated with the power plant, and there may be some constraints on the amount of energy available for the solvent regeneration. Since the regeneration heat supplied to the A-PCC is provided through steam extraction from the power plant, both the flowrate of the exhaust flue gas and requirements on the steam extraction increase when electricity demands increase. Under such a case, an increased amount of flue gas must be handled while the amount of available regeneration heat gets more limited. Scenario 4 investigates the controllability of the process under such operational conditions. In scenario 4, the flue gas flowrate decreases by 20% and then recovers to its nominal value as in scenario 2. However, unlike in scenario 2, the amount of available regeneration heat is limited to 95% of its nominal value after the 400 min mark. Since the desired CO_2 capture rate of 90% or the flash temperature set-point cannot be achieved with the reduced amount of regeneration heat available, some operational problems can be expected to arise when the flue gas flowrate returns to its original value after 500 min.

Fig. 9 shows the dynamic simulation results for scenario 4. First, note that PID1 does not maintain the set-point of 90% CO_2 capture rate and it stays at around 87% after the flue gas flowrate returns to the nominal value. Due to the limited regeneration heat, the CO_2 capture rate shows a slight offset, but the other control variables are maintained at the set-points fairly well. On the other hand, for the PID2 strategy, the solvent flowrate rapidly increases after the 500 min mark due to the unachievable CO_2 capture rate set-point. Also, the flash temperature rapidly decreases and eventually reaches the boiling point of the lean solvent in the flash drum at 791 min mark. Phase separation of the solvent cannot occur in the flash drum at a temperature lower than its boiling temperature, so the operation of the stripper section must be stopped for safety reasons. This is due to the negative RGA pairing. A saturated input is equivalent to opening one of the loops, which leads to instability in the remaining loops. This means that, to control the A-PCC process with the PID2 strategy in the presence of active constraints, additional logics would have to be prepared to deal with input saturations. Finally, if MPC is applied under scenario 4, the off-set in the CO_2 capture rate is also observed like in the PID1 case, but much faster and smoother control results are achieved for all the controlled variables. Since the constraint on the regeneration heat can be easily and directly considered within the MPC algorithm, the operation with the constraint is not a problem for the MPC strategy other than some inevitable offsets once one of the inputs saturates.

4.5. Summary and discussion

Figs. 6–9 show the control results when the RGA and the heuristics based PID control strategies and the MPC strategy are applied to the A-PCC process under different disturbance scenarios. The simulation

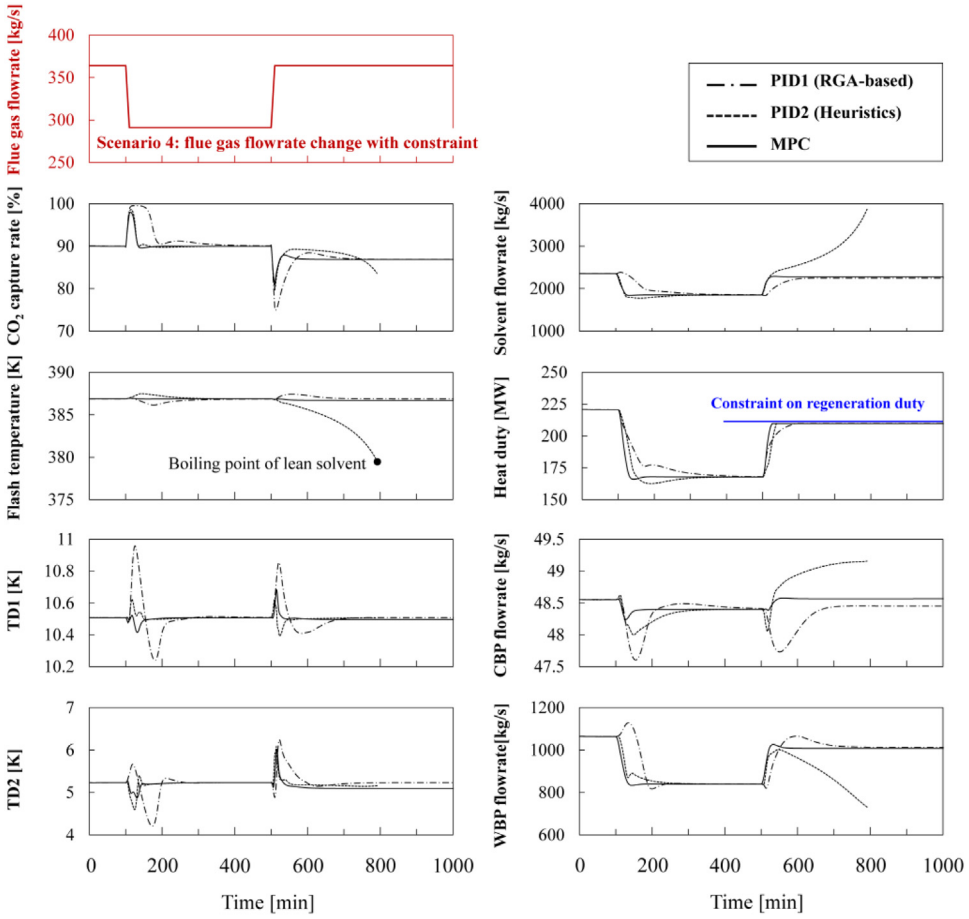

Fig. 9. Closed-loop responses of three control strategies (PID1, PID2, MPC) for scenario 4 (left: control variables; right: manipulated variables).

results consistently demonstrate that MPC delivers superior control performance under all scenarios. The control performances for each control strategy under the different scenarios are quantitatively evaluated using an integrated square error (ISE), which is defined as below:

$$ISE = \sum_{k=0}^{t} (y_k[\%] - y_{SP,k}[\%])^2 \tag{10}$$

where y_k represents the normalized control variables and $y_{SP,k}$ represents the normalized set-point at time k. Table 6 summarizes the calculated ISE values of the three control strategies under the four different scenarios.

For a quick set-point tracking (scenario 1) or disturbance rejection (scenario 2 and 3), MPC and PID2 both show good control performance, especially in controlling the CO_2 capture rate and the flash temperature. Between the two control strategies, the performance of MPC is slightly better than PID2. The major reason for the difference in control performance between PID2 and MPC may be the flash temperature, which has very slow dynamics (see Fig. 5). Since there is a large recycle stream between the absorber and stripper sections, the slow dynamics of the flash temperature also affects other process variables in the absorber section with delays, including the CO_2 capture rate. This is why PID2 shows a prolonged deviation in the CO_2 capture rate, an observation also made in the previous study (Walters, Edgar et al., 2016). With the MPC, however, thanks to its predictive nature, the slow dynamics of the flash temperature can be better handled.

PID1, which is designed based on the RGA analysis, shows poor and sluggish control performance for scenario 1, 2 and 3. Since some pairings of MVs and CVs in the PID1 strategy are physically apart (e.g. $Q_{reg} - \eta_{cap}$ and $F_{solv} - T_{fl}$), it takes significant time for the effect of MVs to reach the CVs, causing the degradation in the control performance. The RGA analysis only reflects the steady-state gains, not dynamical properties such as time constant or dead time, so an RGA-based control strategy can give poor closed-loop dynamics as is the case for PID1.

On the other hand, the problem with negative RGA pairings as in PID2 shows up in the scenario with a constraint. PID2 fails to control the system and diverges at 791 min mark as the saturated input makes one of the loops to act as open loop, causing a sign mismatch. Since the control loop on the flash temperature is opened up when the constraint on the regeneration heat becomes active, the sign of the process gain for the $F_{solv} - T_{fl}$ pairing flips (see also Eq. (5)) and the system

Table 6
Summary of ISE values for four dynamic scenarios.

	CVs	PID1	PID2	MPC
Scenario 1	η_{cap}	7938	3608	2510
	T_{fl}	12 080	12 572	23
	$TD1$	104.6	32.5	14.6
	$TD2$	2369	842	750
Scenario 2	η_{cap}	11 193	2423	1917
	T_{fl}	17 771	17 662	46.3
	$TD1$	787.8	35.3	27.5
	$TD2$	5330	1084	619
Scenario 3	η_{cap}	1077	356	188
	T_{fl}	1218	1776	2.3
	$TD1$	13.7	4.4	3.8
	$TD2$	251	62.5	56.2
Scenario 4	η_{cap}	19 635		11 206
	T_{fl}	21 245	Diverge	13 094
	$TD1$	809		270
	$TD2$	5424		2571

loses the stability. This indicates that, although the slow closed-loop dynamics with the PID1 strategy may reduce the operational flexibility of the process, it can be a better choice than the PID2 strategy. MPC strategy delivers superior control performance compared to the PID-based strategies in all scenarios. Constraints pose no difficulty as such information can be entered into the MPC algorithm explicitly.

One interesting issue is how the linear MPC can show the good control performance in all the tested scenarios. Although the off-set free algorithm is applied in this study, mismatch between the linear model and the nonlinear process can cause a degradation in the control performance when the operating condition changes. The previous work of Jung et al. (2020) provides some insight on this issue since the A-PCC process has similar dynamics with the C-PCC process. When only one input between the CO_2 capture rate and the flue gas flowrate changes, a relatively wide operating range (50%–95% capture rate or 60%–100% flue gas flowrate) can be regulated with a well-tuned linear MPC since the process dynamics do not change by much in such a case. However, if the operating range is further expanded or both the CO_2 capture rate and the flue gas flowrate change simultaneously, model re-linearization or use of a nonlinear MPC may be necessary.

5. Conclusion

A dynamic simulation was performed to present an advanced control strategy appropriate for the energy efficient PCC process equipped with the advanced flash stripper. The operating condition is optimized for energy efficiency by solving an optimization problem, and the dynamic characteristics of the process under such conditions are examined through the step response analysis and the RGA analysis. It is revealed that the A-PCC process has slow dynamic inertia, due to the lean solvent recycle and the warm bypass in the stripper section. In particular, it exhibits complex dynamics such as inverse responses. After an application of PID-based and MPC strategies, it is observed that the PID-based control strategies have limitations in controlling the CO_2 capture rate and the flash temperature due to the slow, interactive dynamics. The proposed MPC strategy delivers good control performance, especially in quick stabilization of the stripper section. It also gives benefits to address operational issues like constraints, showing fast and robust control performance in a dynamic scenario with limited regeneration duty. On the other hand, the PID control strategies showed some shortcomings, either in the speed of regulation or in the handling of constraints. Our simulation results suggest that the application of advanced control techniques such as MPC can help maintain a stable operation with ease as the A-PCC process has to be operated flexibly or becomes constrained due to the integration with the power plant.

Although this study mainly focuses on the A-PCC process and its control using linear MPCs, nonlinear MPCs can potentially be useful for the PCC processes with advanced configurations, especially in the context of flexible operations with the presence of larger disturbances (e.g. co-firing scenario). For example, an application of economic MPC can be a good solution in the flexible operation of an advanced PCC process, as it can simultaneously consider both control and economic benefits. Future research on the process alternatives of PCC process should include not only the steady-state analysis, but also analyses on the process dynamics and a subsequent control strategy suitable for the system.

Declaration of competing interest

The authors declare that they have no known competing financial interests or personal relationships that could have appeared to influence the work reported in this paper.

Acknowledgments

This research was supported by Korea Institute for Advancement of Technology (KIAT) grant funded by the Korea Government (MOTIE) (P0008475, Development Program for Smart Digital Engineering Specialist).

References

Agbonghae, E. O., Hughes, K. J., Ingham, D. B., Ma, L., & Pourkashanian, M. (2014). Optimal process design of commercial-scale amine-based CO2 capture plants. *Industrial and Engineering Chemistry Research*, *53*, 14815–14829.

Bui, M., Fløⁿ, N. E., de Cazenove, T., & Mac Dowell, N. (2020). Demonstrating flexible operation of the technology centre mongstad (TCM) CO2 capture plant. *International Journal of Greenhouse Gas Control*, *93*, Article 102879.

Chan, L. L. T., & Chen, J. (2018). Improving the energy cost of an absorber-stripper CO2 capture process through economic model predictive control. *International Journal of Greenhouse Gas Control*, *76*, 158–166.

Cousins, A., Wardhaugh, L. T., & Feron, P. H. M. (2011). A survey of process flow sheet modifications for energy efficient CO2 capture from flue gases using chemical absorption. *International Journal of Greenhouse Gas Control*, *5*, 605–619.

Dave, N., Do, T., Palfreyman, D., Feron, P. H. M., Xu, S., Gao, S., & Liu, L. (2011). Post-combustion capture of CO2 from coal-fired power plants in China and Australia: An experience based cost comparison. *Energy Procedia*, *4*, 1869–1877.

Decardi-Nelson, B., Liu, S., & Liu, J. (2018). Improving flexibility and energy efficiency of post-combustion CO2 capture plants using economic model predictive control. *Processes*, *6*, 135.

Dubois, L., & Thomas, D. (2018). Comparison of various configurations of the absorption-regeneration process using different solvents for the post-combustion CO2 capture applied to cement plant flue gases. *International Journal of Greenhouse Gas Control*, *69*, 20–35.

El Hadri, N., Quang, D. V., Goetheer, E. L. V., & Abu Zahra, M. R. M. (2017). Aqueous amine solution characterization for post-combustion CO2 capture process. *Applied Energy*, *185*, 1433–1449.

Goto, K., Yogo, K., & Higashii, T. (2013). A review of efficiency penalty in a coal-fired power plant with post-combustion CO2 capture. *Applied Energy*, *111*, 710–720.

He, Z., Sahraei, M. H., & Ricardez-Sandoval, L. A. (2016). Flexible operation and simultaneous scheduling and control of a CO2 capture plant using model predictive control. *International Journal of Greenhouse Gas Control*, *48*, 300–311.

He, X., Wang, Y., Bhattacharyya, D., Lima, F. V., & Turton, R. (2018). Dynamic modeling and advanced control of post-combustion CO2 capture plants. *Chemical Engineering Research and Design*, *131*, 430–439.

Heo, S., & Daoutidis, P. (2016). Control-relevant decomposition of process networks via optimization-based hierarchical clustering. *AIChE Journal*, *62*, 3177–3188.

Heo, S., Jogwar, S. S., Rangarajan, S., & Daoutidis, P. (2014). Graph reduction of complex energy-integrated networks: Process systems applications. *AIChE Journal*, *60*, 995–1012.

Hikita, H., Asai, S., Ishikawa, H., & Honda, M. (1977). The kinetics of reactions of carbon dioxide with monoethanolamine, diethanolamine and triethanolamine by a rapid mixing method. *The Chemical Engineering Journal*, *13*, 7–12.

Hossein Sahraei, M., & Ricardez-Sandoval, L. A. (2014). Controllability and optimal scheduling of a CO2 capture plant using model predictive control. *International Journal of Greenhouse Gas Control*, *30*, 58–71.

Jung, H., Im, D., Heo, S., Kim, B., & Lee, J. H. (2020). Dynamic analysis and linear model predictive control for operational flexibility of post-combustion CO2 capture processes. *Computers & Chemical Engineering*, *140*, Article 106968.

Jung, J., Jeong, Y. S., Lee, U., Lim, Y., & Han, C. (2015). New configuration of the CO2 capture process using aqueous monoethanolamine for coal-fired power plants. *Industrial and Engineering Chemistry Research*, *54*, 3865–3878.

Kent, L. R., & Elsenberg, B. (1976). Better data for amine treating.

Koytsoumpa, E. I., Bergins, C., & Kakaras, E. (2018). The CO2 economy: Review of CO2 capture and reuse technologies. *The Journal of Supercritical Fluids*, *132*, 3–16.

Li, K., Cousins, A., Yu, H., Feron, P., Tade, M., Luo, W., & Chen, J. (2016). Systematic study of aqueous monoethanolamine-based CO2 capture process: model development and process improvement. *Energy Science & Engineering*, *4*, 23–39.

Li, K., Leigh, W., Feron, P., Yu, H., & Tade, M. (2016). Systematic study of aqueous monoethanolamine (MEA)-based CO2 capture process: Techno-economic assessment of the MEA process and its improvements. *Applied Energy*, *165*, 648–659.

Liang, Z., Gao, H., Rongwong, W., & Na, Y. (2015). Comparative studies of stripper overhead vapor integration-based configurations for post-combustion CO2 capture. *International Journal of Greenhouse Gas Control*, *34*, 75–84.

Lin, Y.-J., Madan, T., & Rochelle, G. T. (2014). Regeneration with rich bypass of aqueous piperazine and monoethanolamine for CO2 capture. *Industrial and Engineering Chemistry Research*, *53*, 4067–4074.

Luu, M. T., Abdul Manaf, N., & Abbas, A. (2015). Dynamic modelling and control strategies for flexible operation of amine-based post-combustion CO2 capture systems. *International Journal of Greenhouse Gas Control*, *39*, 377–389.

Mac Dowell, N., & Shah, N. (2013). Identification of the cost-optimal degree of CO2 capture: An optimisation study using dynamic process models. *International Journal of Greenhouse Gas Control*, *13*, 44–58.

Mechleri, E., Lawal, A., Ramos, A., Davison, J., & Dowell, N. M. (2017). Process control strategies for flexible operation of post-combustion CO2 capture plants. *International Journal of Greenhouse Gas Control*, *57*, 14–25.

Montañés, R., Fløⁿ, N., & Nord, L. (2017). Dynamic process model validation and control of the amine plant at CO2 technology centre mongstad. *Energies*, *10*, 1527.

Muchan, P., Saiwan, C., Narku-Tetteh, J., Idem, R., Supap, T., & Tontiwachwuthikul, P. (2017). Screening tests of aqueous alkanolamine solutions based on primary, secondary, and tertiary structure for blended aqueous amine solution selection in post combustion CO2 capture. *Chemical Engineering Science*, *170*, 574–582.

Nittaya, T., Douglas, P. L., Croiset, E., & Ricardez-Sandoval, L. A. (2014). Dynamic modelling and control of MEA absorption processes for CO2 capture from power plants. *Fuel*, *116*, 672–691.

Notz, R., Mangalapally, H. P., & Hasse, H. (2012). Post combustion CO2 capture by reactive absorption: Pilot plant description and results of systematic studies with MEA. *International Journal of Greenhouse Gas Control*, *6*, 84–112.

Oh, H.-T., Ju, Y., Chung, K., & Lee, C.-H. (2020). Techno-economic analysis of advanced stripper configurations for post-combustion CO2 capture amine processes. *Energy*, *206*, Article 118164.

Panahi, M., & Skogestad, S. (2012). Economically efficient operation of CO2 capturing process. Part II. Design of control layer. *Chemical Engineering and Processing: Process Intensification*, *52*, 112–124.

Patron, G. D., & Ricardez-Sandoval, L. (2020). A robust nonlinear model predictive controller for a post-combustion CO2 capture absorber unit. *Fuel*, *265*, Article 116932.

Pinsent, B. R. W., Pearson, L., & Roughton, F. J. W. (1956). The kinetics of combination of carbon dioxide with hydroxide ions. *Transactions of the Faraday Society*, *52*, 1512–1520.

Rezazadeh, F., Gale, W. F., Lin, Y.-J., & Rochelle, G. T. (2016). Energy performance of advanced reboiled and flash stripper configurations for CO2 capture using monoethanolamine. *Industrial and Engineering Chemistry Research*, *55*, 4622–4631.

Rochelle, G. T., Wu, Y., Chen, E., Akinpelumi, K., Fischer, K. B., Gao, T., Liu, C.-T., & Selinger, J. L. (2019). Pilot plant demonstration of piperazine with the advanced flash stripper. *International Journal of Greenhouse Gas Control*, *84*, 72–81.

Salvinder, K. M. S., Zabiri, H., Taqvi, S. A., Ramasamy, M., Isa, F., Rozali, N. E. M., Suleman, H., Maulud, A., & Shariff, A. M. (2019). An overview on control strategies for CO2 capture using absorption/stripping system. *Chemical Engineering Research and Design*, *147*, 319–337.

Schmid, C., & Biegler, L. T. (1994). Quadratic programming methods for reduced hessian SQP. *Computers & Chemical Engineering*, *18*, 817–832.

Skogestad, S. (2000). Plantwide control: the search for the self-optimizing control structure. *Journal of Process Control*, *10*, 487–507.

Taylor, R., & Krishna, R. (1993). *Multicomponent mass transfer*. New York, NY (United States): John Wiley and Sons, Inc., None.

Walters, M. S., Edgar, T. F., & Rochelle, G. T. (2016). Regulatory control of amine scrubbing for CO2 capture from power plants. *Industrial and Engineering Chemistry Research*, *55*, 4646–4657.

Walters, M. S., Osuofa, J. O., Lin, Y.-J., Edgar, T. F., & Rochelle, G. T. (2016). Process control of the advanced flash stripper for CO2 solvent regeneration. *Chemical Engineering and Processing - Process Intensification*, *107*, 21–28.

Wu, X., Shen, J., Li, Y., Wang, M., Lawal, A., & Lee, K. Y. (2018). Nonlinear dynamic analysis and control design of a solvent-based post-combustion CO_2 capture process. *Computers & Chemical Engineering*, *115*, 397–406.

Wu, X., Wang, M., Liao, P., Shen, J., & Li, Y. (2020). Solvent-based post-combustion CO2 capture for power plants: A critical review and perspective on dynamic modelling, system identification, process control and flexible operation. *Applied Energy*, *257*, Article 113941.

Zhang, S., Shen, Y., Wang, L., Chen, J., & Lu, Y. (2019). Phase change solvents for post-combustion CO2 capture: Principle, advances, and challenges. *Applied Energy*, *239*, 876–897.

Zhang, Q., Turton, R., & Bhattacharyya, D. (2016). Development of model and model-predictive control of an MEA-based postcombustion CO2 capture process. *Industrial and Engineering Chemistry Research*, *55*, 1292–1308.

Zhang, Q., Turton, R., & Bhattacharyya, D. (2018). Nonlinear model predictive control and H∞ robust control for a post-combustion CO2 capture process. *International Journal of Greenhouse Gas Control*, *70*, 105–116.